# Surface heat loss assessment of geothermal fields in the TVZ, using remote sensing and terrestrial techniques

Anya Seward[1], Robert Reeves[1], Nick Macdonald[1] and Chris Bromley[1]

[1]GNS Science, Wairakei Research Centre, Private Bag 2000, Taupo 3352

a.seward@gns.cri.nz

**Keywords:** *Heat loss, thermal infrared, remote sensing, Karapiti, Waimangu, Waiotapu, Rotorua.*

**ABSTRACT**

Assessment of surface heat loss in geothermal areas can provide information and insight into the size and character of underlying geothermal resources. It also provides a method to monitor changes to a geothermal system and assess geothermal hazards related to movement of subsurface steam. Additionally, variations in fluid flow pathways may result in changes of geothermal feature characteristics and fluid discharge at the surface.

This paper presents findings from heat loss assessments at several geothermal areas within the Taupo Volcanic Zone, including Karapiti (part of the Wairakei-Tauhara geothermal system), Waimangu geothermal valley, Waiotapu Geothermal Field, and Rotorua Geothermal Field. Methods for surface heat loss determination include, direct heat flux measurements using a water-based calorimeter, inferred heat flux assessments from temperature-depth relations, spring and stream flow assessments, and inferred heat fluxes from remote aerial thermal infrared (TIR) and satellite TIR assessments. This paper will compare results and findings from these surveys.

## 1. INTRODUCTION

Areas of steaming ground originate from discharges of geothermal vapour through the surface. The steam heats the groundwater, interacts with rainfall, and can transfer large amounts of thermal energy. Accurately quantifying and monitoring such heat-loss is difficult and can be time-consuming and expensive. However, heat-loss data is becoming ever more important for calibrating and advising reservoir models. This paper describes research work being undertaken to improve the quantification of heat-loss assessments using remote TIR techniques and ground-based temperature and calorimetry measurements.

The initial study was undertaken at Karapiti (Craters of the Moon), within the Wairakei-Tauhara Geothermal System. This site comprised mostly of steaming ground, and varying vegetation ground-cover. Here, ground-based measurements were collected, in conjunction with aerial TIR data. These datasets were also compared to Satellite TIR collected by Landsat-8 (Bromley et al, 2015; Seward et al, 2018).

The second study was located at Waimangu Geothermal Valley, the southern margin of the Waimangu-Rotomahana-Tarawera geothermal system. This is an area of confined geothermal activity, mostly located within the valley. Here two large geothermal lakes are present, Frying Pan Lake and Inferno Crater Lake, along with several small springs located along the Waimangu Stream, which flow down the middle of the valley. Several small areas of steam heated ground are also present amongst stunted vegetation growth. At this location, methodologies were advanced to include evaporative heat loss from the lakes, and mass discharge along the stream (Seward et al 2022a).

In this paper, we also present preliminary results from Waiotapu Geothermal Field and several geothermally active areas of Rotorua City. These sites add additional complexities to the determination of surface heat loss, which are discussed in the following text.

## 2. METHODS

One key objectives of these studies is to be able to accurately assess surface heat loss using remote sensing methodologies. We therefore explore and compare heat loss assessments from both terrestrial based datasets and methodologies, with remotely collected dataset, primarily airborne TIR.

There are several means with which heat is lost to the atmosphere within geothermal environments, including hot springs, geysers, hot pools, mud pools, heated and steaming ground, and fumaroles. The heat loss from fumaroles have not been analysed in the terrestrial based studies and have been treated as steaming ground in the aerial TIR analysis. We recognize that this is a short fall in both of these methodologies. Additionally, heat loss through steam to the atmosphere at dynamically active springs and geysers is also not satisfyingly accounted for in either methodology, with the terrestrial base analysis treating these features as flowing springs (with no evaporative component) and the aerial TIR analysis treating these features as static pools rather than dynamic flowing features.

### 2.1 Terrestrial based methods

There are several components to considered in determining heat loss for a geothermal area. They include heat loss to the atmosphere (1) from heat transferred through heated ground (section 2.1.1), (2) from geothermal water bodies, including surface hot pools, and springs (section 2.1.2), and also (3) from heat transferred into streams through subsurface seeps, springs, and also surface flows accumulated in streams (section 2.1.3).

#### 2.1.1 Heat loss through the ground

Two methods have been used to calculate a surface heat flux from the ground, one using a water-based calorimeter to measure a heat flux, and the other using temperature depth profiles to determine a heat flux. In order to get a total heat loss for a geothermal area, sites are selected to represent a predefined ground-cover type. An average heat flux for ground-cover class is determined. A vegetation / ground-cover map of the area is created using recent aerial images, to which an average heat flux for each ground cover class is applied to produce a total heat loss for the area.

##### *2.1.1.1 Calorimeter method*

Firstly, heat flux measurements were made using a water-based calorimeter (Hochstein and Bromley, 2005; Seward et al 2018). The calorimeter records linear increases in


ISSN 2703-4275

temperature of water, starting from near-ambient conditions, caused by steady ground heat transfer over, for example, a 5-minute period. This allows a total heat flux from the surface to be determined. Increase in water temperature while the calorimeter is slightly elevated (on a 2 cm ring) over a similar period of time (5 minutes) allows the non-conductive (radiation and convection) heat flux from the surface to be determined. Before, after, and in-between ground and elevated measurements, the calorimeter is left on a thick wooden block to measure the background influence of the surrounding atmosphere (at ambient temperature). Temperatures on the lid of the calorimeter are also continuously recorded to allow correction, if necessary, for ambient temperature changes. Figure 1 shows an example of the recorded temperature in the water-filled calorimeter over a total site occupation period of about 30 minutes.

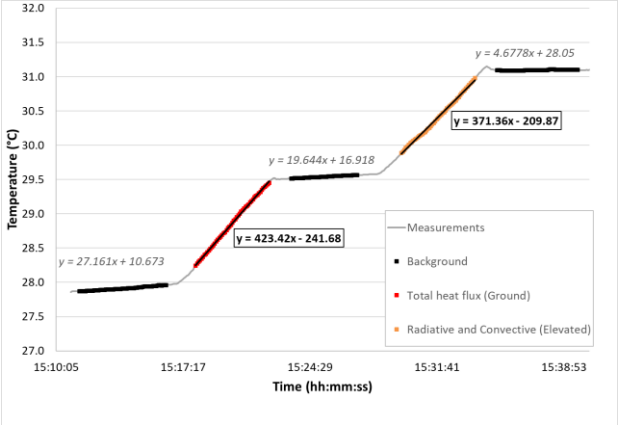


**Figure 1: Example of calorimeter data measurements used to calculate heat flux at a measurement site.**

The total heat flux from the ground is determined from the temperature gradient with time ($\frac{\Delta T_g}{\Delta t}$) measured while the equipment is placed directly on the surface, and multiplying it by the mass of the water within the calorimeter ($m$), and the specific heat capacity of water ($c$), divided by the total area ($A$) of ground covered by the calorimeter.

$$q_{tot} = \frac{mc\left(\frac{\Delta T_g}{\Delta t} - \frac{\Delta T_{lid}}{\Delta t}\right)}{A} \quad \textbf{(EQ 1)}$$

where $\frac{\Delta T_{lid}}{\Delta t}$, is the change in temperature recorded by the lid sensor over time and is used as a proxy for any heating / cooling influence from the ambient air temperature.

*2.1.1.2 Temperature-depth Profiles*

Heat flux based on ground temperature-depth profiles is calculated using a method described by Seward et al. (2018), where the depth at which boiling temperatures are reached are determined and converted into a heat flux. The depths to boiling points are either measured directly when $Z_{BP}$ is less than 1 m or inferred from extrapolating a fitted exponential function to the temperature-depth data.

$$Z_{BP} = exp[c_1(T_{BP} - T_z)] \quad \textbf{(EQ 2)}$$

Where $T_z$ is the temperature at depth $Z$, $T_{BP}$ is the temperature at which boiling occurs at atmospheric pressure (i.e. T = 98.6°C), and $c_1$ is a constant derived by Hochstein and Bromley (2005) at the Karapiti geothermal area (–0.025).

Heat flux is then calculated from the boiling point depth using the following power-law relationship (Hochstein and Bromley 2005).

$$q_{ZB} = a\left[\frac{Z_{BP}}{Z_0}\right]^{-b} \quad \textbf{(EQ 3)}$$

Where $a$ and $b$ are empirically derived constants ($a$ = 148 $Wm^{-2}$; $b$ = 0.84; Seward et al. 2018), and $Z_0$ is a normalised depth (1 m).

2.1.2 Heat loss from water features

We use the methods developed by Dawson (1964) and converted to SI units by Sorey and Colvard (1994), to calculate a heat loss from a water body. There are four key mechanisms for heat loss from water bodies to consider when calculating a heat loss. They are evaporation ($Q_E$), conduction (QC), Radiation ($Q_R$) and direct mass flow ($Q_S$). Dawson developed the following set of empirical equations to determine each component (in kW).

$$Q_E = 0.001 * A\left(h_{s,tp} - h_{w,tp}\right)(0.0065 + 0.0029w)\frac{(P_{H2O,tp} - P_{H2O,atm})}{P_{ATM}} \quad \textbf{(EQ 4)}$$

Where A is the area of the pool ($m^2$), $h_{s,tp}$ is the enthalpy of the steam at pool temperature ($t_p$) ($Jkg^{-1}$), $h_{w,tp}$ is the enthalpy of water at pool temperature ($Jkg^{-1}$), $w$ is the wind speed ($m\ s^{-1}$), $P_{H2O,tp}$ is the vapour pressure of water at $t_p$ (bar), $P_{H2O,atm}$ is the atmospheric vapour pressure (bar) and $P_{ATM}$ is the average annual atmospheric pressure in bar.

The heat loss by conduction and molecular diffusion, $Q_C$, is related to $Q_E$ by the Bowen ratio, RB (Sutton 1953).

$$RB = \frac{Q_C}{Q_E} = 6.1 \times 10^{-4} P_{tot} \frac{(t_p - t_{atm})}{(P_{H2O,tp} - P_{H2O,atm})} \quad \textbf{(EQ 5)}$$

where $t_{atm}$ is the atmospheric temperature in °C.

$$Q_R = 0.001 * A\varepsilon\sigma(T_P^4 - T_{atm}^4) \quad \textbf{(EQ 6)}$$

where ε is emissivity, equal to 0.955 for water, σ is the Stefan-Boltzman constant equal to 5.68 x $10^{-8}$ $Wm^{-2}K^{-4}$, and $T_P$ and $T_{amt}$ refer to the temperature of the pool ($P$) and ambient air ($amt$) temperature in Kelvin.

Heat loss from flowing springs and overflow of pools can be determined by:

$$Q_S = 0.001 M_w(h_w - h_{atm}) \quad \textbf{(EQ 7)}$$

where $M_w$ is the mass flow of heated water in $kgs^{-1}$, $h_w$ is the enthalpy of the discharging water in $KJkg^{-1}$ and $h_{atm}$ is the enthalpy of water at the atmospheric temperature in $KJkg^{-1}$ (Sorey and Colvard 1994).

Therefore, the total heat loss ($Q_{WB}$ (MW)) is represented by:

$$Q_{WB} = 0.001 \times (Q_E + Q_C + Q_R + Q_S) \quad \textbf{(EQ 8)}$$

2.1.3 Heat loss to streams

Two methods for determining the heat flow within a stream are used to determine heat loss through surface discharge.

1. Heat loss (MW) determined from the enthalpy of stream water (calculated from stream temperatures) and flow rate ($V$)

$$Q_T = \frac{H_T V}{1000} \quad \textbf{(EQ 9)}$$


ISSN2703-4275

Where $H_T$ is the enthalpy of the stream at measured temperature ($T$) (KJ/kg) and $V$ is the measure flow rate of the stream (kg/s).

2. Heat loss (MW) calculated from the determined chloride flux ($F_{Cl}$) and the enthalpy of the deep geothermal water associated with 1 g of Cl (MJ/g) (Glover 1992; Bibby et al 1995a).

$$Q_{Cl} = F_{Cl} H_{Cl} \quad \textbf{(EQ 10)}$$

### 2.2 Aerial Thermal Infrared

Thermal infrared (TIR) data is easier to collected than terrestrial datasets. They are collected at night (or early hours of the morning, pre-sunrise), using a FLIR A615 TIR camera mounted to either a fixed wind aircraft or helicopter. The collected images were mosaicked and georegistered to aerial photography. Inferred surface temperatures are calculated per pixel by applying a calibration equation derived from measured water temperatures at known locations collected at the time of the flight.

Initially, three methods were used to calculate a heat loss (Bromley et al., 2015). A preferred method using a direct empirical relationship between inferred TIR temperatures and heat flux:

$$Q_{TIR} = 50.3*(T_{(inferred)} - T_{(ambient)}) - 148 \text{ W/m}^2 \quad \textbf{(EQ 11)}$$

To determine the total heat loss for a given area the heat flux is multiplied by the pixel area (generally < 1m$^2$). Inferred surface temperatures are calculated by determining a linear relationship between measured surface temperatures and TIR signal values, over a representative temperature range of the area being surveyed. This relationship is unique for each survey and each location.

## 3. RESULTS AND DISCUSSION

Heat losses from four different geothermal fields are presented and discussed here. The approaches vary slightly from site to site as advances in methodology are made as each field increases in complexity. The Karapiti geothermal areas within the Wairakei-Tauhara geothermal system was our initial test site for comparing terrestrial based heat loss measurements to remote TIR techniques. It also included attempts to use satellite TIR imagery, but it was found that the spatial resolution and temperature differential were insufficient to determine accurate heat loss (Bromley et al, 2015; Seward et al 2018). The methods were then applied to Waimangu and Waiotapu Geothermal Fields, where dynamic thermal discharge from steaming water bodies and streams needed consideration. And finally, Rotorua, where anthropogenic influences and infrastructure also need to be considered.

The following sections present and compare the results and methods used at each site.

### 3.1 Karapiti

The Karapiti geothermal area (also known as Craters of the Moon), located within the Wairakei-Tauhara geothermal system at Taupo (New Zealand), was the initial site for testing the relationship between terrestrial based heat loss analysis and remote sensing techniques (Seward et al 2018). The area covers roughly 350m$^2$, containing mostly heated or steaming ground and eruption craters. There are no water bodies within the area, so mass heat flow is not considered in this assessment. Additionally, fumaroles and actively steam plumes are not assessed in these studies.

Thermal infrared data (Figure 2) was collected in February 2014, using a FLIR A615 TIR camera mounted to an Aero Commander 680F fixed-wing aircraft. Shallow ground temperature-depth profiles (< 1m) and water-based calorimeter measurements were collected at 15 locations during the week prior to the TIR flight. Terrestrial site selection was based on differing ground-cover and safe access (Figure 3). Many sites had previously been used as heat flux measurements sites (e.g. Mia et al 2012).

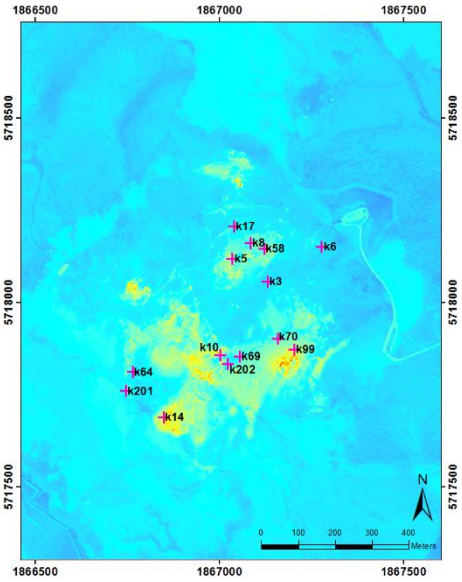


**Figure 2: TIR image of Karapiti. Locations of terrestrial measurements are shown by the pink crosses. Yellow-Red colours show warmer inferred surface temperatures, while bluer colours indicate cooler surface temperatures**

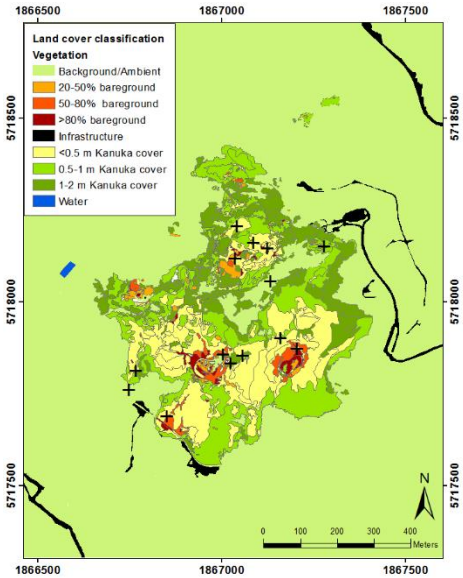


**Figure 3: Ground-cover classification map of Karapiti.**

Table 1 presents the total heat loss from the Karapiti geothermal area (Seward et al., 2018).


ISSN2703-4275

**Table 1: Results from heat loss assessments at Karapiti (Seward et al 2018).**

| | Heat loss (MW) |
|---|---|
| **TIR Results** | |
| $Q_{TIR}$ for land pixels T>18°C only | 49 |
| **Terrestrial Results** | |
| $Q_{tot}$ | 47.6 |
| $Q_{ZB}$ | 58.2 |

The results from these three methods are in relatively close agreement, with an ~20% discrepancy between the two terrestrial based methods. This is likely caused by not all heat being transported in the subsurface (detected by temperature-depth profiles) is actually emitted at the surface and detected by the calorimeter. This is likely to be enhanced in areas of steam heat ground, such as much of the ground at Karapiti.

### 3.2 Waimangu

The Waimangu Geothermal Field is located at the southern end of the Tarawera rift zone in the central North Island. Most of the surface geothermal activity is confined within a valley, which contains 2 large geothermal pools, Frying Pan Lake and Inferno Crater Lake. There are several springs and small geysers along the Waimangu Stream, and small areas of heated and steaming ground.

Thermal infrared data was collected in January 2017, using a FLIR A615 TIR camera mounted on a fixed wing aircraft (Figure 4; Reeves and Macdonald, 2017). Shallow ground temperature-depth profiles and water-based calorimeter measurements were made at 24 sites in the Waimangu geothermal valley between February and March 2017 (Seward et al 2022). These sites spanned are range of differing ground cover (Figure 5).

Table 2 list the total determined heat loss from the TIR data, terrestrial measurement, and stream gauging. In this assessment, only the evaporative heat loss ($Q_E$) from the lake surfaces were calculated. Mass flow from Frying Pan Lake outflow and springs were determined by gauging the Waimangu Stream at the outflow of Frying Pan Lake and at a site located downstream of most of the geothermal activity and prior to flowing into the lake (Figure 5). It is important to note that these measurements were taken when Inferno Crater was not overflowing.

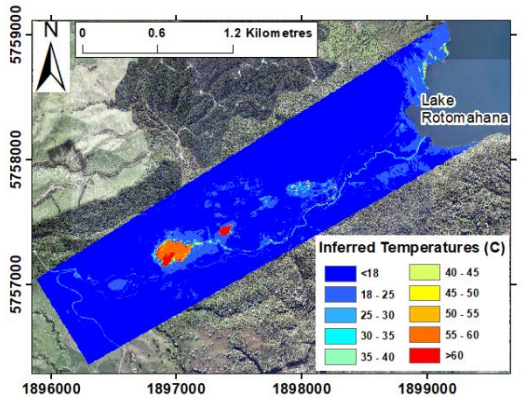


**Figure 4 TIR image of the Waimangu geothermal valley. Yellow-Red colours show warmer inferred surface temperatures, while bluer colours indicate cooler surface temperatures**

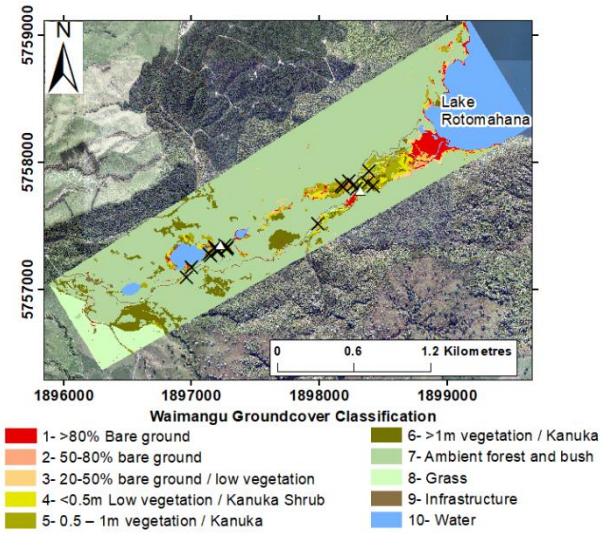


**Figure 5: Ground cover classification map of the Waimangu geothermal valley, with terrestrial measurement sites indicated by the black "X".**

**Table 2: Results from Heat loss assessments at Waimangu geothermal field.**

| | Heat loss (MW) |
|---|---|
| **TIR Results** | |
| $Q_{TIR}$ for land pixels T>18°C only | 87 |
| $Q_E$ from $T_{TIR_INF}$ | 106 |
| **Terrestrial Results** | |
| $Q_{tot}$ | 107 |
| $Q_{ZB}$ | 74 |
| $Q_E$ | 60 |
| $Q_T$ (downstream-upstream) | 142 |
| $Q_{Cl}$ (downstream-upstream) | 187 |

The results presented in Table 2, suggest that a total heat loss for the Waimangu Valley (excluding the flow within Waimangu stream) determined from TIR data totals ~193MW, and ~167MW from terrestrial calorimeter and evaporative loss from the lakes. Note that the heat loss determined from calorimeter here is higher than that determined from the temperature-depth profiles. It is thought that this discrepancy could be due to the warm air temperatures at the time of measurements, or differing geological conditions, that might require further investigations into the appropriateness of the $c_1$ determined for Karapiti. This will require further work to determine and is planned as further data are collected at different geothermal sites.

Additionally, a large discrepancy is seen between $Q_E$ determined from terrestrial measurements at from TIR inferred surface temperatures. We believe that the terrestrial water temperature measured at the outflow of Frying Pan Lake is not representative of the water surface temperature of the full lake. Figure 4 shows that there is a clear heat source at the far end of the Lake. A large amount of this heat is mixed with the lake; however, a large portion is lost to the atmosphere through stream prior to mixing. Therefore, the measured water temperature at the outflow point is a minimum water temperature rather than an average for the Frying Pan Lake.


ISSN2703-4275

### 3.3 Waiotapu

The Waiotapu Geothermal Field is located approximately 30 km SE of Rotorua (New Zealand) and approximately 7 km south of Waimangu Geothermal Field. It is the considered the largest of the 20 major fields in the TVZ, ~17km$^2$, based on the extend of known geothermal surface features. The area contains over 500 features which include hot springs, pools, mud pools and areas of heated and steaming ground.

TIR data was collected over Waiotapu in April, 2019, with a terrestrial based survey undertaken in January/February 2020 (Reeves and Sanders 2019; Seward et al 2022b). The terrestrial based survey included 11 calorimeter and temperature-depth profiles, and 19 stream gauging sites (Figure 6).

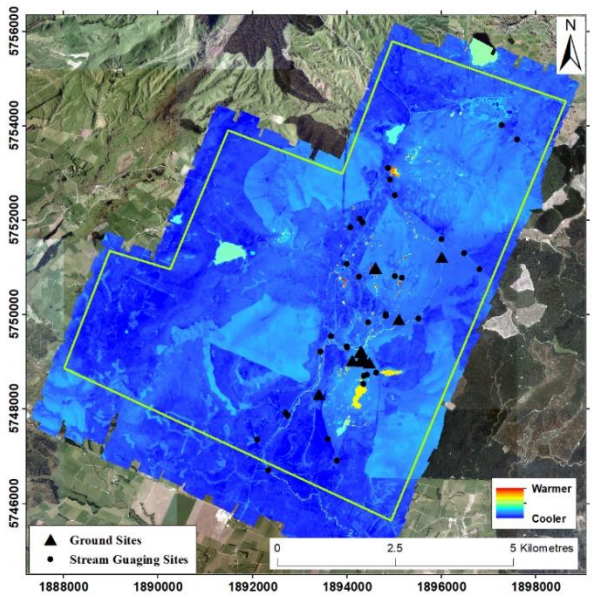


**Figure 6: Collected TIR data over Waiotapu. Warmer temperatures shown in reds, ambient temperatures in blues. Black circles show stream gauging and sampling locations. Black Triangles show locations of calorimeter/Temperature-depth profile measurement sites. Green out-line show the boundary for heat loss calculation.**

A ground cover map has not yet been created for Waiotapu, so a total heat loss through the ground from terrestrial method has not yet been determined. However, based on the TIR data, 90% of surface heat loss is lost from the water features, with only 10% being emitted from the ground surface. This is not unreasonable, as much to the surface area is farmland or forested. Within the Wai-O-Tapu Thermal Wonderland, where the majority of the geothermal surface features are found, much of the ground is either forested, vegetated, or silica sinter, all of which have near ambient heat fluxes (measured with the Calorimeter; Seward et al 2022b). The amount of steaming or heated ground in the areas is minimal, suggested that the majority of the heat is transferred through water flow and mostly confined to the pools and springs that discharge into the Waiotapu Stream.

Heat loss from the pools were calculated using an average inferred surface temperature from the TIR data per pool rather than per pixel (as was done in the Waimangu study). Table 3 lists the total surface heat loss determined from the TIR data and stream gauging. $Q_E$, $Q_C$ and $Q_R$ are determined for all the pools in the area and summed to a total heat loss from water bodies $Q_{WB}$. It is interesting to note that $Q_{TIR}$ for all pixels greater that 18°C calculated using EQ 11, 353.7MW, is in close agreement with $Q_{WB}$ + $Q_{TIR}$ (land pixels), 328.1MW, a difference of 7%.

**Table 3: Results from Heat loss assessments at Waiotapu Geothermal Field.**

| | **Heat loss (MW)** |
|---|---|
| **TIR Results** | |
| $Q_{TIR}$ for all pixels T>18°C | 353.7 |
| $Q_{TIR}$ for land pixels T>18°C only | 37.5 |
| $Q_E$ from $T_{TIR_INF}$ | 177.8 |
| $Q_C$ from $T_{TIR_INF}$ | 56.8 |
| $Q_R$ from $T_{TIR_INF}$ | 56.0 |
| $Q_{WB}$ (surface discharge $Q_S$ not determined) | **290.6** |
| **Terrestrial Results** | |
| $Q_T$ (Waiotapu outflow – inflow) | 142 |
| $Q_{Cl}$ (Waiotapu outflow – inflow) | 187 |

A total heat loss for the Waiotapu Geothermal Field is determined by summing $Q_{TIR}$ (land only), $Q_{WB}$ and $Q_{Cl}$ to give a total of ~515MW.

### 3.4 Rotorua

Rotorua City is built around an activity geothermal system. The larger Rotorua Geothermal System covers an area of approximately 18-28 km$^2$ and includes several areas of active surface activity around the city and geothermal seeps into Lake Rotorua. This study focusses on assessing surface heat loss from the 2014 TIR survey, primarily focused on the Kuirau Park and Government Gardens areas (Reeves et al. 2014).

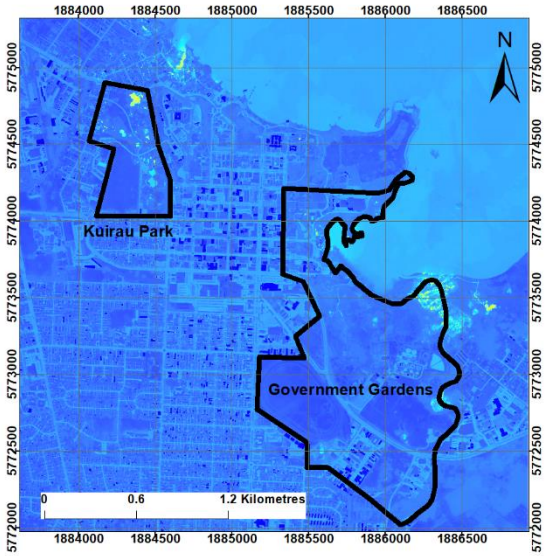


**Figure 7: TIR image of the Rotorua. Black polygons show the extent of the heat loss analysis for focused on Kuirau Park and Government Gardens. Yellow-Red colours show warmer inferred surface temperatures, while bluer colours indicate cooler surface temperatures**

Heat loss from the geothermal pools were calculated using the average inferred surface temperatures determined from the TIR data.

In 2018, a comprehensive terrestrial based heat loss assessment of several of the active geothermal areas in


ISSN2703-4275

Rotorua was undertaken (Seward et al, 2020). Terrestrial data collected from pools during the 2018 survey are used to re-calculate the heat loss from pool, using a constant average air temperature of 17°C and assumed windspeed of 1m/s. This air temperature corresponds to the average air temperature over the days of data collection, while the assumed windspeed is the same windspeed as assumed for the other assessments in this paper. The results are therefore a fraction of the results published previously from this study (Seward et al 2018, 2020). 37 geothermal pools are assessed at Kuirau Park, while 12 are assessed at Government Gardens / Sulphur Bay. Heat loss through the ground in these two areas have previously published as 6.62MW from Government gardens / Sulphur Bay area, and 0.77MW at Kuirau Park.

**Table 4: Results from Heat loss assessments at Kuirau Park**

| ***Kuirau Park*** | **Heat loss (MW)** |
|---|---|
| **TIR Results** | |
| $Q_{TIR}$ for land pixels T>18°C only | 3.4 |
| $Q_E$ from $T_{TIR_INF}$ | 7.2 |
| $Q_{WB}$ (surface discharge $Q_S$ not determined) | 10.5 |
| Total heat loss ($Q_{TIR}+Q_{WB}$) | **13.9** |
| **Terrestrial Results** | |
| $Q_E$ | 6.5 |
| $Q_C$ | 1.1 |
| $Q_R$ | 1.3 |
| $Q_{WB}$ | 8.9 |
| $Q_{tot}$ (ground loss) | 0.8 |
| Total heat loss ($Q_{tot}+Q_{WB}$) | **9.7** |

**Table 5: Results from Heat loss assessments at Government Gardens & Sulphur Bay**

| ***Government Gardens & Sulphur Bay*** | **Heat loss (MW)** |
|---|---|
| **TIR Results** | |
| $Q_{TIR}$ for land pixels T>18°C only | 29.5 |
| $Q_E$ from $T_{TIR_INF}$ | 2.7 |
| $Q_{WB}$ (surface discharge $Q_S$ not determined) | 3.9 |
| Total heat loss ($Q_{TIR}+Q_{WB}$) | **33.3** |
| **Terrestrial Results** | |
| $Q_E$ | 1.0 |
| $Q_C$ | 0.2 |
| $Q_R$ | 0.3 |
| $Q_{WB}$ | 1.5 |
| $Q_{tot}$ (ground loss) | 6.6 |
| Total heat loss ($Q_{tot}+Q_{WB}$) | **8.1** |

It is important to note that the heat loss assessment using the TIR data covered a much larger area, particularly around Government Gardens and Sulphur Bay, than the 2018 terrestrial survey did. There are many areas of high heat flow in Sulphur Bay that are unsafe to measure on the ground. Additionally, there was 4 years between the TIR and the terrestrial survey, which will account for some of the differences in results. Of note, is that at the time of the terrestrial survey, water levels, and flow rates of pools were anomalously low.

## 4. DISCUSSION & CONCLUSION

Many of the techniques used in these investigations rely on observed relationships and empirically derived equations from data and observations at the Wairakei Geothermal Field (Dawson 1964; Hochstein and Bromley 2005; Bromley et al 2011). These methods and equations have then been applied, tested and adapted at other geothermal fields (e.g., Seward et al 2022). Results from these investigations suggest that the derived methods are applicable to other locations and provide results that are in agreement with historic heat loss estimates (Bibby et al 1995b).

This paper has presented and summarised 8 years of research looking at developing a robust methodology to accurately determine surface heat loss from remote sensing. Results have shown that total heat loss from geothermally active areas determined from differing techniques are in close agreement with one another. However, there is still work to be done in quantifying uncertainty associated with each method.

Calorimetry provides spot measurement of heat flux from the ground. These measurements have been shown to have a 10% reproducibility rate at Karapiti in the dry seasons (Hochstein and Bromley, 2005). Uncertainties are introduced when integrating these heat flux measurements over an area, based on ground-cover type. This relationship between ground-cover and heat flux is not new and has been used since the mid-1960's (Dawson and Dickinson, 1970). Errors are introduced when producing the ground-cover map. These maps are currently created by using recent aerial photographs of the area of interest, and visually creating polygons of area containing different vegetation types. There is a large amount of human bias in this approach, which is then amplified when integrating spot heat flux measurements over these areas. New techniques are being investigated to minimise the human bias, by utilising hyperspectral techniques for lithology mapping (e.g. Rodrigues-Gomez et al 2021).

Thermal Infrared methodology seems to overcome this issue by calculating inferred surface temperatures, which are then used to determine a heat flux per pixel. This method removes the need for extensive ground-cover mapping, however, will still need the water bodies mapped so that evaporative heat flux can be calculated separately using the appropriate equations.

Results of heat loss from water bodies show good correlation between terrestrial based water temperature measurements and inferred TIR temperature measurement approaches for most geothermal pools. It is clear that in the cases of the larger hotter pools, like Frying Pan Lake, that remote techniques allow more accurate evaporative heat loss assessments. Terrestrial temperature measurements are limited in access points and in the case of Frying Pan Lake, the heat source is at the far end of the lake, and the mixing of hot and cold water is not consistent. Additionally, the surface temperatures near the heat source are high resulting in evaporation, prior to any mixing of hot and cool water.

There are, however, some limitations to the remote sensing techniques as well. The key limitation is that dynamic heat loss, e.g., flowing discharges, can not be assessed remotely. These need to be measured directly through flow gauging techniques. Additionally, in areas where steam is present, true surface temperatures may be masked, resulting in incorrect inferred surface temperatures.

However, from the investigations undertaken so far, if appears that the remote TIR technique coupled with measured ground temperatures and flow gauging, may provide the best technique for heat loss assessment of geothermal areas. Further investigations will continue with the datasets already collected to confirm the TIR conversion equations is appropriate for all locations.


ISSN2703-4275

**ACKNOWLEDGEMENTS**

We would like to acknowledge the "New Zealand Geothermal Future" GNS Science core research funding [contract C05X1702], Contact Energy Ltd, Department of Conversation, Waimangu Geothermal Valley, Ngati Whoa Runanga Trust, Wai-O-Tapu Thermal Wonderland, and numerous land owners who allows terrestrial measurements to be undertaken.

**REFERENCES**

Bibby, H.M, Glover, R.B., and Whiteford, P.C., (1995a). The heat outout of the Waimangu, Waiotapu-Waikite and Reporoa Geothermal systems (NZ): Do Chloride Fluxes provide an accurate meaure?, Proceedings 17th NZ Geothermal Workshop 1995.

Bibby, H. M., Caldwell, T. G., Davey, F. J., & Webb, T. H. (1995b). Geophysical evidence on the structure of the Taupo Volcanic Zone and its hydrothermal circulation. *Journal of volcanology and geothermal research*, *68*(1-3), 29-58.

Bromley, C.J. and Hochstein, M.P.: Thermal properties of steaming ground (Wairakei Field, NZ). Proc. 23rd New Zealand Geothermal Workshop, Auckland, New Zealand, pp.69-74, (2001).

Bromley, C.J., van Manen, S.M., Mannington, W., (2011). Heat flux from steaming ground: reducing uncertainties. In: Proceedings of 36th Stanford Workshop on Geothermal Reservoir Engineering. Stanford University, California. pp. 925–931.

Bromley, C.J., Ashraf, S., Seward, A., and Reeves, R., 2015 Monitoring and quantifying heat loss from significant geothermal geothermal areas via remote sensing. Proc. 37th New Zealand Geothermal Workshop, Taupo, New Zealand, (2015)

Dawson GB. 1964. The nature and assessment of heat flow from hydrothermal areas. New Zealand Journal of Geology and Geophysics. 7(1):155-71. doi:10.1080/00288306.1964.10420167.

Dawson, G.B., and Dickinson, D.J., (1970), Heat Flow studies in Thermal Areas of the North Island of New Zealand, *UN Symposium on the Development and Utilization of Geothermal Resources, Pisa 1970 Geothermics-special issue 2*, 466-473.

Glover, R.B., 1992, Integrated heat and mass discharge from Rotorua geothermal system. Geothermics, 21(1-2), pg 89-96

Hochstein, M.P. and Bromley, C.J.: Measurement of heat flux from steaming ground. *Geothermics*, 34(2): pp.133-160, (2005).

Mia, M.B., Bromley, C.J., Fujimitsu, Y.: Monitoring heat flux using Landsat TM/ETM + thermal infrared data : a case study at Karapiti ('Craters of the Moon') thermal area, New Zealand. *Journal of Volcanology and Geothermal Research*, 235/236: pp.1-10, (2012).

Reeves, R.R., Scott, B.J., and Hall, J., 2014, 2014 Thermal Infrared survey of the Rotorua and Lake Rotokawa-Mokoai Geothermal Fields, GNS Science Report 214/57.28p

Reeves, R., Macdonald, N. (2017) Aerial Thermal Infrared Survey of the Waimangu-Rotomahana – Mt Tarawera Geothermal Field. Lower Hutt (NZ): GNS Science. *GNS Science report; 2017/48*. 20p.

Reeves R, Sanders F. 2019. 2019 Thermal infrared survey of the Waiotapu Geothermal Field. Wairakei (NZ): GNS Science. 22 p. (GNS Science report; 2019/57). doi:10.21420/ZD6D-GD88.

Rodrigues-Gomez, C., Kereszturi, G. Reeves, R., Rae, A., Pullanagari, R., Jeyakumar, P., Procter, J., 2021. Lithological mapping of waiotapu Geothermal Field (New Zealand) using hyperspectrual and thermal remote sensing and ground exploration techniques. Geothermics, 96, 2021. doi.org/10.1016/j.geothermics.2021.102195

Seward, A.M., Ashraf, S., Reeves, R. and Bromley, C., 2018 Improved environmental monitoring of surface geothermal features through comparisons of thermal infrared, satellite remote sensing and terrestrial calorimetry, *Geothermics*, 73, 60-73

Seward, A., Reeves, R., Doorman, P., Sanders, F., Lor, S., MacDonald, N., Brakenrig, T., Graham, D., 2020, Surface heat loss assessment of Rotorua Geothermal Field, In proceedings New Zealand Geothermal workshop 2020.

Seward, A., Reeves, R., Alcaraz, A., 2022a, Assessment of the Surface heat loss from Waimangu Geothermal Valley: Comparison of terrestrial based assessments techniques with remote sensing, Journal of Volcanology and Geothermal Research, 430, doi.org/10.1016/j.jvolgeores.2022.107630

Seward AM, Brakenrig T, Macdonald N, Shanks, J. 2022b. Collection and initial assessment of terrestrial heat flux of the Waiotapu Geothermal Field. Lower Hutt (NZ): GNS Science. 79 p. (GNS Science report; 2022/07). doi:10.21420/ECCP-E459.

Sorey ML, and Colvard EM. 1994. Measurements of heat and mass flow from thermal areas in Lassen Volcanic National Park, California, 1984-93. Menlo Park (CA): U.S. Geological Survey. 35 p. (Water-resources investigations report; 94-4180-A).

Sutton PM. 1953. Variation of the elastic constants of crystalline aluminium with temperature between 63°K and 773°K. Physical Review. 91(4):816-821. doi:10.1103/PhysRev.91.816.